Semiclassical study of particle motion in two-dimensional and three-dimensional elliptical boxes. II

1987 J. Phys. A: Math. Gen. 20 1115

(http://iopscience.iop.org/0305-4470/20/5/023)

J. Phys. A: Math. Gen. 20 (1987) 1115-1136. Printed in the UK

Semiclassical study of particle motion in two-dimensional and three-dimensional elliptical boxes: II

Robert Arvieu† and Yves Ayant‡

† Institut des Sciences Nucléaires, 38026 Grenoble Cédex, France
‡ Laboratoire de Spectrométrie Physique, BP 87, 38402 St Martin d'Hères Cédex, France

Received 11 March 1986, in final form 25 June 1986

Abstract. The spectrum of an ellipsoidal box of prolate and oblate symmetry are calculated by an exact diagonalisation and by semiclassical methods. The influence of a separatrix in phase space is analysed with the help of the WKB phases derived in an earlier paper. Differences between the prolate and oblate $L_z = 0$ states are explained using this separatrix. It is found that the EBK method, improved by the uniform approximation, leads to a spectrum in very good agreement with the wave mechanical results. The spectrum of a two-dimensional elliptical membrane ('billiard' box) is also studied with similar conclusions.

1. Introduction

In a recent article (Carbonell *et al* 1985) the classical dynamics of a particle in the spherical average field of a nucleus has been analysed. Limiting cases were considered (harmonic oscillator, infinite spherical well) as well as potentials of the Woods-Saxon type (more precisely the Buck-Pilt version). The geometrical properties of the classical energy-action surface were studied in connection with the EBK semiclassical method of quantisation. The most significant features of the single particle spectrum were explained by local properties of this surface and their evolution with particle number. All the cases treated share a common property: the uniformity of the topology of the classical phase space. This topology can be characterised by the nature of classical caustics; the caustics of the spherical potential relevant to nuclear physics are in general two circles (or spheres) which mark the limit of the radial motion. Therefore in the semiclassical limit the details of the spectrum and also to some extent the main features of the wavefunction (for example the domain where it oscillates) are simply connected to the features of the energy-action surface. The introduction of corrections of higher order in $\hbar$ introduces only tiny corrections which are not interpretable by using only semiclassical mechanics to lowest order.

The situation is much more complex if we deform the above potentials. For the sake of simplicity we will restrict the discussion to the case where the deformation is such that the equipotentials are prolate or oblate ellipsoids.

(i) The deformed harmonic oscillator is the case of maximum simplicity: the potential is still integrable, the semiclassical energies are exact and the topology of the caustics is unique. It can readily be seen that the energy-action surface, for each specific value of L_z, the projection of the angular momentum on the axis of symmetry, is a plane that moves as a function of deformation. It is the motion of this plane that explains the shift of the single particle levels with energy.

0305-4470/87/051115+22$02.50

The harmonic oscillator is the only one in which the phase space changes monotonously with the parameters and where the equation of the trajectories can be written simply. For the other potentials it will be convenient to distinguish the planar trajectories with $L_z = 0$ which are contained in meridian planes of the ellipsoids from the non-planar ones which will not be considered in this paper.

(ii) The ellipsoidal cavity with infinite well will be the main object of our study. The discussion of this case has been prepared by an earlier paper by Ayant and Arvieu (1987, hereafter referred to as I). Its interest lies in the fact that its topology is not uniform. Indeed the phase space is divided into two regions by a separatrix. These regions evolve differently with the deformation: one decreases in size while the second increases. Our intention is to discuss quantitatively how this separatrix manifests itself in the spectrum; more specifically, how it helps to explain the oblate-prolate differences when it is properly combined with the motion of the energy-action surface with deformation.

(iii) The case of the Buck-Pilt potential is much more involved, as was shown by Carbonell (1983) and discussed in Carbonell *et al* (1984). Indeed this potential is non-integrable. However it has been found (Carbonell 1983) that in a large region of the parameter space the phase space is divided into two regions by a separatrix which is topologically identical to that of the ellipsoidal cavity. In that region semiclassical quantisation is possible and the ellipsoidal cavity provides a useful system for comparison. It turns out that the energy spectrum of a deformed Buck-Pilt potential is very similar to that of the cavity, apart from small but essential modifications like the level repulsion. It seems that the high degree of complexity of the classical dynamics—bifurcations, chaos, etc—contributes only to the explanation of these modifications. Therefore it is our conclusion that the main differences between the oblate and the prolate spectra are found in the discussion of the ellipsoidal cavity.

Since we found it necessary to discuss the barrier effects for the 'billiard', the numerical discussion will also be presented for completeness.

2. Determination of the separatrix

We will use the same notation as in Ayant and Arvieu (1987). The semi-axes of the ellipsis in which the classical motion takes place are called $R_\rangle$ and $R_\langle$ and the focal distance $2f$. The ratio

$$\mu = R_\rangle / R_\langle \tag{1}$$

will be used as our deformation parameter in the interval (1, 2) for which the consideration of the ellipsoidal deformations is the most significant. Our intention is to follow the spectrum as a function of μ. It is conventional in nuclear physics to impose a volume conservation. Therefore, if R_0 is the radius of the spherical nucleus the condition for a prolate nucleus is

$$R_\rangle R_\langle^2 = R_0^3 \tag{2}$$

and for an oblate nucleus, it becomes

$$R_\rangle^2 R_\langle = R_0^3. \tag{3}$$

In this manner $R_\rangle$, $R_\langle$ and f have a different variation in a prolate or oblate nucleus. In a prolate nucleus

$$R_\rangle = R_0 \mu^{2/3} \qquad R_\langle = R_0 \mu^{-1/3} \tag{4}$$

while in the oblate nucleus

$$R_> = R_0 \mu^{1/3} \qquad R_< = R_0 \mu^{-2/3}. \tag{5}$$

With this convention the ellipses corresponding to oblate and prolate nuclei of the same μ have different semi-axes.

The two-dimensional case is treated in the same spirit, i.e. we use conservation of the surface

$$R_> R_< = R_0^2. \tag{6}$$

The single particle energy is written as $k^2/2m$ and we will use $\hbar = 1$. The classical action integrals are defined in the elliptic coordinates η, ξ and the separation constant E as

$$I_\eta = \frac{1}{\pi} \int_{\eta_0}^{\eta_1} kf(\cosh^2 \eta - (E/kf)^2)^{1/2} \, \mathrm{d}\eta \tag{7}$$

$$I_\xi = \frac{1}{\pi} \int_{\xi_0}^{\pi - \xi_0} kf((E/kf)^2 - \cos^2 \xi)^{1/2} \, \mathrm{d}\xi. \tag{8}$$

The value of η_1 is related to the eccentricity of the boundary by

$$\eta_1 = \cosh^{-1} R_>/f. \tag{9}$$

We have two limiting cases:

(1) elliptic caustics

$$\eta_0 = \cosh^{-1} \sqrt{E}/kf \qquad \xi_0 = 0 \tag{10}$$

(2) hyperbolic caustics

$$\eta_0 = 0 \qquad \xi_0 = \cos^{-1} \sqrt{E}/kf. \tag{11}$$

The integrals (7) and (8) are combinations of elliptic integrals; their expressions can be found in Keller and Rubinow (1960). Since η_0 or ξ_0, calculated from (10) and (11), define caustics homofocal to the boundary we can write I_η and I_ξ in the general form

$$I_\eta = kf\mathcal{T}_\eta(e, e_0) \tag{12}$$

$$I_\xi = kf\mathcal{T}_\xi(e, e_0) \tag{13}$$

where the $\mathcal{T}$ are functions of the eccentricities of the boundary e and of the caustics e_0. We can also write the following inequalities after inspection of the integrals:

(a) $e_0 < 1$

$$0 \leqslant I_\eta < kf\mathcal{T}_\eta(e, 1) = \pi^{-1} kf(e^{-1} - 1) \tag{14}$$

$$kf\mathcal{T}_\xi(e, 1) < I_\xi \leqslant kf\mathcal{T}_\xi(e, e). \tag{15}$$

This last inequality can be written in terms of a complete integral of the first kind $E(\frac{1}{2}\pi, e)$:

$$2kf/\pi < I_\xi \leqslant \pi^{-1} E(\tfrac{1}{2}\pi, e). \tag{16}$$

(b) $e_0 > 1$

$$kf\mathcal{T}_\eta(e, 1) < I_\eta \leqslant kf\mathcal{T}_\eta(e, \infty) \tag{17}$$

$$0 \leqslant I_\xi < kf\mathcal{T}_\xi(e, 1). \tag{18}$$

The value $e_0 = 1$ corresponds to the particular values of the actions

$$(I_\eta)_S = \pi^{-1} k_S (e^{-1} - 1) f \tag{19}$$

$$(I_\xi)_S = 2k_S f/\pi. \tag{20}$$

The scaling properties expressed in the forms (12) and (13) indicate that, e being given, e_0 is a function of the ratio I_η/I_ξ. On the other hand, (19) and (20) help to find the eccentricity e_S of the box for which the states labelled by I_η and I_ξ are found on the separatrix

$$e_S = \frac{I_\xi}{2I_\eta + I_\xi} \tag{21}$$

while (20) enables us to write $k_S f$ right away as

$$k_S f = \frac{\pi}{2I_\xi}. \tag{22}$$

Equations (21) and (22) form the central part of the discussion of this paper. It helps to find immediately whether $e_0 < 1$ or $e_0 > 1$.

Suppose that I_η and I_ξ are given and e_S is calculated with (21).
If $e < e_S$ we have

$$\frac{I_\eta}{I_\xi} < \left(\frac{I_\eta}{I_\xi}\right)_S \qquad \text{and} \qquad e_0 < 1.$$

If $e > e_S$ we have

$$\frac{I_\eta}{I_\xi} > \left(\frac{I_\eta}{I_\xi}\right)_S \qquad \text{and} \qquad e_0 > 1.$$

This shows that if a state labelled by I_η and I_ξ is followed adiabatically as a function of e (or μ) it has first a circular caustic when $e = 0$; it becomes elliptic when μ increases, it crosses the separatrix e_S given by (21) and ends up with a hyperbolic caustic for $e > e_S$.

(a) Prolate case: the simplest discussion of the separatrix is given for the prolate case for which we have established in I that

$$I_\eta = n + \tfrac{3}{4} \qquad I_\xi = l + \tfrac{1}{2}. \tag{23, 24}$$

Using these values we find the corresponding value of e_S by (21) and of μ_S by $1/(1-e_S^2)^{1/2}$ as

$$\mu_S = \frac{2(2n+l+2)}{[(4n+4l+5)(4n+3)]^{1/2}}. \tag{25}$$

Let us consider all the states of same l. The values of μ_S found by this formula are lower for the higher n. On the other hand, if we fix the radial quantum number n, μ_S is higher for the high l. Table 1 provides a numerical illustration of that property for a subset of orbits which are occupied in heavy nuclei like Pb.

The s states present the remarkable property that μ_S is so small that the caustics are certainly hyperbolic for values of μ appropriate to deformed nuclei. At the other extreme the 1f, 1g, 1h, 1i, etc, orbitals are associated with high values of μ_S. The picture thus obtained is that in a prolate nucleus we must associate the single particle states of low angular momentum with a classical motion with a hyperbolic caustic; on

Table 1. The variation of μ_S with l for fixed radial quantum number.

	Prolate	Oblate		
Label	EBK 1 μ_S	EBK 1 μ_S	EBK 0 μ_{Se}	EBK 0 μ_{Sh}
1s	1.033	1.078	1.033	1.155
2s	1.008	1.018	1.008	1.033
3s	1.003	1.008	1.003	1.014
4s	1.002	1.004	1.002	1.008
5s	1.001	1.003	1.001	1.005
1p	1.155	1.100	1.155	1.061
2p	1.048	1.033	1.048	1.021
3p	1.024	1.016	1.024	1.010
4p	1.014	1.010	1.014	1.006
1d	1.281	1.377	1.281	1.512
2d	1.100	1.125	1.100	1.155
3d	1.053	1.065	1.052	1.078
4d	1.033	1.040	1.033	1.048
1f	1.400	1.316	1.400	1.25
2f	1.155	1.072	1.155	1.107
3f	1.085	1.047	1.085	1.061
1g	1.512	1.637	1.512	1.809
2g	1.209	1.243	1.209	1.281
3g	1.120	1.136	1.120	1.154
1h	1.616	1.512	1.616	1.429
2h	1.263	1.231	1.263	1.203
1i	1.715	1.863	1.715	2.065
2i	1.316	1.355	1.316	1.400
1j	1.809	1.688	1.809	1.591

the other hand the orbitals with a high angular momentum should be associated with an elliptic caustic.

Figure 1 illustrates the variation of e_0 with μ calculated by the semiclassical method. This confirms the universal behaviour described above. It is noteworthy that formula (25) does not separate the families of even l from those with odd l. This identity was explained in I.

(b) Oblate case: (i) primitive WKB (EBK 0). We recall the definition of α, utilised in I:

$$\alpha = \frac{k^2 f^2 - E'}{2kf} \tag{26}$$

where E' is a fictitious energy which appears through the variable separation process. One is far from the crossing of the separatrix when $|\alpha| \gg 1$; $\alpha > 0$ means a hyperbolic caustic, $\alpha < 0$ means an elliptic caustic.

In these limits, paper I gives the quantisation conditions (the primitive WKB ones):

$$\alpha < 0 \qquad I_\eta = n + \tfrac{3}{4} \qquad I_\xi = l + \tfrac{1}{2} \tag{27}$$

$$\alpha > 0 \qquad \begin{cases} I_\eta = n + \tfrac{1}{2} & I_\xi = l + 1 \quad (\text{even } l) \quad (28) \\ I_\eta = n + 1 & I_\xi = l \quad (\text{odd } l). \quad (29) \end{cases}$$

It is worth noting that (27) is identical with (23) and (24) found in the prolate case.

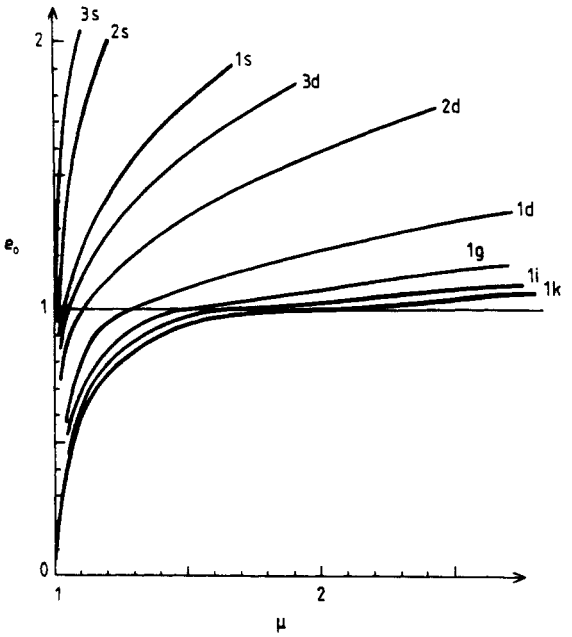

Figure 1. Eccentricities e_0 of semiclassical states of the prolate cavity as a function of μ. For clarity the curves are not drawn in the vicinity of $\mu = 1$ since for all of them $e_0 \to 0$.

When we are looking for the box eccentricity e_S such that an (n, l) state stands on the separatrix using equation (21), we must choose one of the preceding rules, either (27) which leads to μ_{Se}, or (28) and (29) which lead to μ_{Sh} whose expression depends on parity of l. On account of the remark concerning (27) μ_{Se} is identical to μ_S given by (25). On the other hand we obtain

$$\mu_{Sh}^{+} = \frac{2n+l+2}{[(2n+1)(2n+2l+3)]^{1/2}} \qquad \text{(even } l\text{)} \tag{30}$$

$$\mu_{Sh}^{-} = \frac{2n+l+2}{[(2n+2)(2n+2l+2)]^{1/2}} \qquad \text{(odd } l\text{).} \tag{31}$$

The different values of μ_S for the oblate case illustrate one of the well known shortcomings of the primitive WKB rules that we formulate as follows:

$$\text{if } 1 < \mu < \mu_{Se} \text{ there is an elliptic caustic} \tag{32}$$

$$\text{if } \mu_{Sh} < \mu \text{ there is a hyperbolic caustic.} \tag{33}$$

However in the even-l case $\mu_{Se} < \mu_{Sh}$. Therefore in the corresponding interval (μ_{Se}, μ_{Sh}) there are simply no solutions of the coupled WKB equations for the variables η and ξ! In contrast, in the odd-l case $\mu_{Se} > \mu_{Sh}$ we have an opposite situation and therefore in the interval (μ_{Sh}, μ_{Se}) the solution with hyperbolic caustic always exists and that with elliptic caustic still exists! There are two candidates with different energies which correspond to one level.

These deficiencies are known (Ford *et al* 1959) to be relieved by the uniform approximation where μ_{Se} and μ_{Sh} coincide.

Since the primitive WKB rules exaggerate the even-odd l differences in the oblate case, it is interesting to calculate the eccentricities e_0 one obtains using these rules. Figure 2 contains this effect for the 1p and 1d states. It is important to note that when $e_0 < 1$ the eccentricity of the elliptic caustic is the same for prolate and oblate cavities of identical μ as well as the value of kf. The 1p and 1d states have a quite similar character in the prolate case of $e_0 > 1$. However the slopes are rather different in the oblate case. This interesting effect, which is also found with the uniform approximation, is obtained despite the mentioned shortcomings of the primitive WKB method.

(ii) Uniform approximation (EBK 1): the deficiencies of EBK 0 of leading to two possible μ_S disappear if one uses the phase of the EBK solution corresponding to $\alpha = 0$. That phase $\beta(\alpha)$ obeys a curious symmetry law:

$$\beta(\alpha)+\beta(-\alpha)=2\beta(0). \tag{34}$$

Equation (34) is derived from (85) and (87b) of I; $\beta(\alpha)$ is expressed with the help of $\beta_A(\alpha)$ and $\beta_S(\alpha)$, plotted on figure 1 of I; these functions obey (34). (It may be of interest to note that such symmetry results from the parabolic shape of the top of the barrier. Analogous calculations with another shape (e.g. $-C(x^4)$ give a phase which does not obey (34)). Hence the quantisation conditions for I_ξ and I_η are obtained by taking the mean value of the cases $\alpha = \pm\infty$:

$$I_\eta = n+\tfrac{5}{8} \qquad I_\xi = l+\tfrac{3}{4} \qquad \text{(even } l\text{)} \tag{35}$$

$$I_\eta = n+\tfrac{7}{8} \qquad I_\xi = l+\tfrac{1}{4} \qquad \text{(odd } l\text{)}. \tag{36}$$

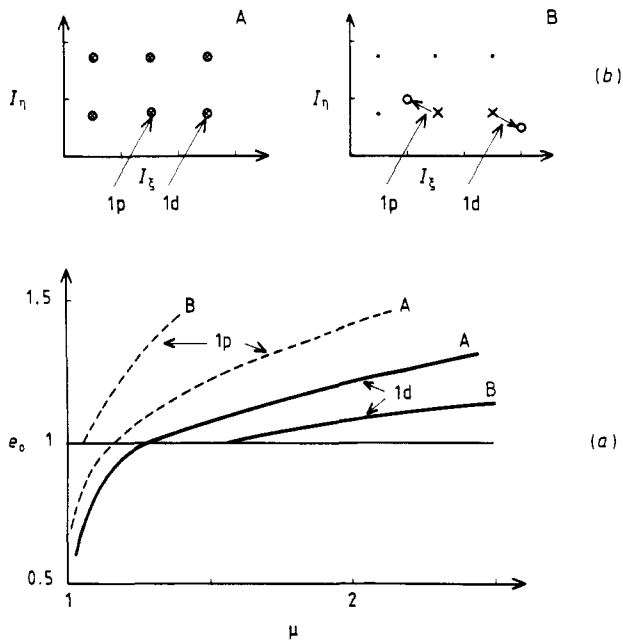

Figure 2. (*a*) Eccentricities e_0 of the semiclassical states 1p and 1d calculated in the primitive WKB method for oblate (B) and prolate (A) cavities as a function of μ; (*b*) values of the action integrals, the circle corresponding to elliptic caustics, the cross to hyperbolic caustics. Note the discontinuities of the action for the oblate case.

We obtain the following expressions of μ_S:

$$\mu_S^+ = \frac{2(2n+l+2)}{[(4n+4l+\frac{11}{2})(4n+\frac{5}{2})]^{1/2}} \tag{37}$$

$$\mu_S^- = \frac{2(2n+l+2)}{[(4n+4l+\frac{9}{2})(4n+\frac{7}{2})]^{1/2}}. \tag{38}$$

The following inequalities are found when comparing the oblate and prolate cases for the same n and l:

$$\mu_S \text{ prolate} < \mu_S^+ \text{ oblate} \qquad \text{for even } l \tag{39}$$

$$\mu_S \text{ prolate} > \mu_S^- \text{ oblate} \qquad \text{for odd } l. \tag{40}$$

The motion with elliptic caustics persists for higher deformation in the oblate nucleus for even l; it is confined to a smaller interval of deformation for the odd-l case.

(c) Elliptic 'billiard': the discussion there is very similar to that of the oblate case. The symmetric case plays the same role as the even-l case and the antisymmetric one that of the odd-l state. Since this case is of little interest for nuclear physics the formulae for μ_S, μ_{Se}, μ_{Sh} are not given here but can be easily worked out using (21) and the proper WKB phases in the quantisation rules or those of the uniform approximation according to the rules given above and in I.

3. Quantum and semiclassical spectra

In order to obtain, with good precision, all the single particle energies which are important in heavy nuclei, we have used the following method. By a scaling transformation, different for the long and short axes of the ellipses, the boundary is transformed into a circle or a sphere. A basis of cylindrical or spherical Bessel functions which have zeros on the boundary are used to diagonalise the kinetic energy which contains an anisotropic term. The matrix elements of this term are simpler expressions of the zeros of cylindrical or spherical Bessel functions. Details are given in the appendix. This method was first used by Moszkowski (1955).

3.1. The cavity

The energy spectrum of the even states of the cavity is plotted in figure 3. The value of $(kR_0)^2$ is plotted instead of $(kf)^2$ and the states are labelled as l_{n+1}. This spectrum has the overall character of a deformed Woods-Saxon potential. However there is a general behaviour which is followed by all the states but with a rate that depends upon n and l. The single particle energy has a local maximum for $\mu = 1$ and one local minimum for each sign of the deformation. Typical cases are $2_2, 4_2, 2_3, 6_2$. However sometimes the three extrema are nearly equal to 1 and the chosen scale shows only a minimum $(0_1, 0_2, \ldots 0_n)$ or is such that the minimum is outside the figure (as for $4_1, 6_1, \ldots l_1$). For a few states the arrows indicate μ_S for the prolate case and the two values μ_{Se} and μ_{Sh} for the oblate case. These arrows indicate the places, or the regions, where a change of curvature occurs in the single particle energy curve.

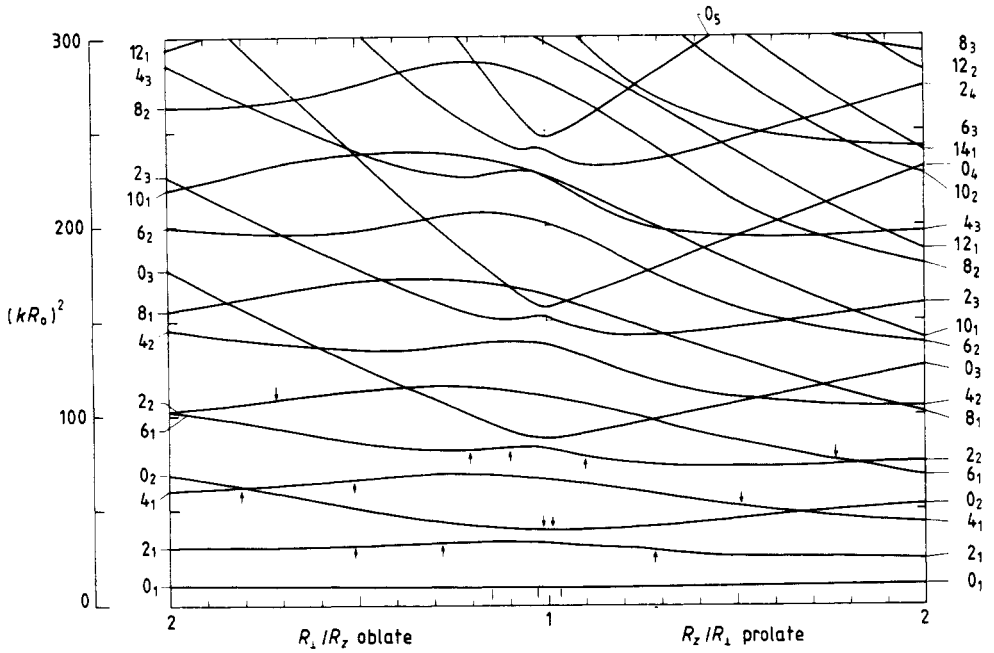

Figure 3. The complete quantum energy spectrum of the prolate and oblate cavities up to $(kR_0)^2 = 300$. Only positive parity states are drawn. The arrows indicate the values of μ_S (prolate), μ_{Se} and μ_{Sh} (oblate) of table 1 for a few long-lying states. States are labelled as l_{n+1}.

Figure 4 shows the single particle spectrum $n = 1$ and $0 \leq l \leq 8$ where the even parity states are plotted beside the odd ones. The arrows now indicate the location of μ_S given by (25), (28) and (31). One sees here a striking property. The prolate spectrum is smooth as far as the dependence in l is concerned. The odd-l levels can be smoothly interpolated from the even-l case. The situation there is entirely different in the oblate case where the odd levels cross the even. This behaviour can be traced to the difference in the barrier effects for even and odd states. Indeed the barrier has a maximum for $\xi = \pi/2$ which separates two minima. A similar difference in the spectrum is also found for a Buck-Pilt potential as found out by Touchard (1985). It is represented in figure 5.

In order to provide a more complete investigation of this even-odd effect let us compare the spectra of an oblate cavity to that of a prolate one each for $\mu = 1.5$. (All the single particle states in the energy region are considered.) It is important to see that the density of states exhibits a large difference: there are 43 states in the prolate nuclei and only 26 in the oblate ones. This number characterises the well known fact that the $L_z = 0$ states lie higher in energy in the oblate system. This effect is amplified by the fact that the odd states lie even higher.

The semiclassical method explains almost entirely this behaviour, even in the frame of the primitive WKB method. The energy spectrum with this method can be seen in figure 6. On the other hand, in figure 7 the quantum value of $(kR_0)^2$ for the 1g level is shown for comparison with the EBK 0 and EBK 1 values. The EBK 0 shortcoming for the oblate case is obvious here. The uniform method EBK 1 provides better energies in general and is able to fill the gap between the separatrix S_e and S_h. In spite of the fact that the vertical scale used in figure 7 slightly amplifies the disagreement of the

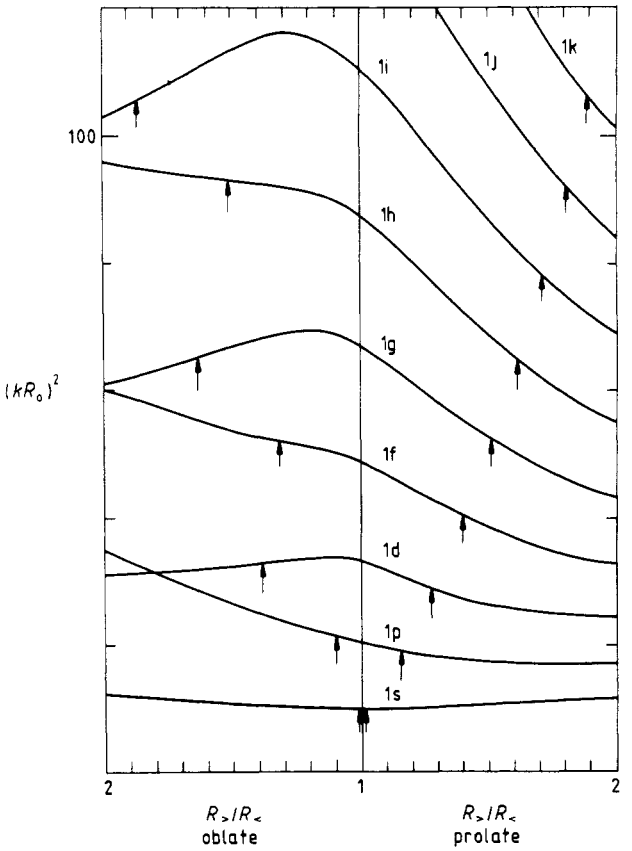

Figure 4. The quantum energy levels of all states $n = 1$ of the cavity. The arrows indicate the values of μ_S (equation (25)) for the prolate cavity, (30) and (31) for the oblate.

primitive WKB method the only region where the uniform approximation is needed absolutely is the interval (μ_{Se}, μ_{Sh}).

Figure 8 is the plot of $\mathcal{T}_\eta(e, e_0)$ and $\mathcal{T}_\xi(e, e_0)$ defined in (12) and (13) from the integrals (7) and (8). It is indeed simple to represent a section of the energy-action surface at a constant energy. Only the prolate situation is analysed there. The arrows indicate the directions in which the lattice points are located. For a given μ the point e_0 is found by the intersection of the represented curve and a straight line drawn out from the arrow. The behaviour of every single particle level is explained by noting the coordinates of different intersection points. A general behaviour is observed: the surface leaves regions of high I_η for the regions of high I_ξ when μ increases. The separatrix is represented as a dotted line. For example the 2g state is very near to its separatrix for $\mu = 1.2$ (1.209 from table 1).

Most of the structure of the spectrum is explained by the curvature and the displacement of the energy-action surface and by the scales of the actions.

There are, finally, small disagreements between EBK 1 and the quantum spectrum. To our knowledge it is difficult to explain them qualitatively in a semiclassical language. Table 2 illustrates in a quantitative way the difference between the semiclassical results and the quantum ones. Typically the differences are 0.5% in this table as well as for most of the levels considered in this paper for the 'billiard' as well as the cavity.

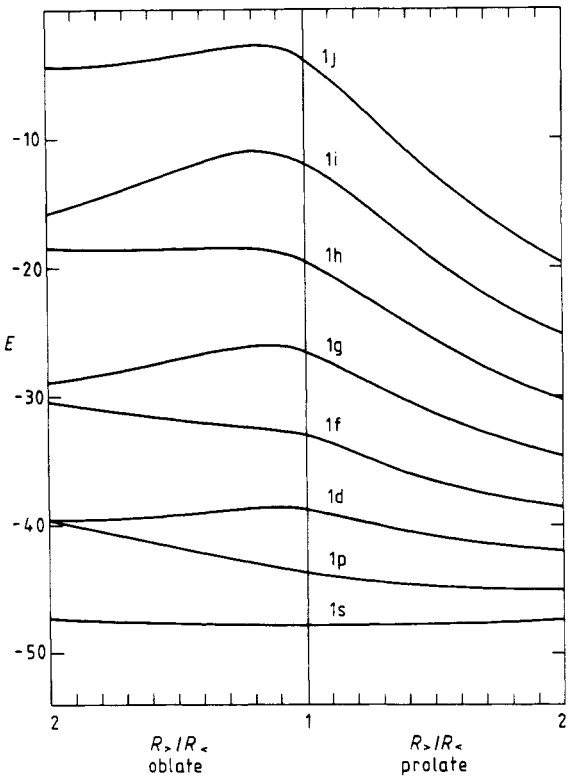

Figure 5. Same as in figure 4, but where the cavity is replaced by a Buck-Pilt potential which takes an ellipsoidal deformation (from Touchard 1985). The energy scale is in MeV.

3.2. The 'billiard'

As previously stated, this case has been done for completeness. Results were already given by Keller and Rubinow (1960) for a single value of the deformation $\mu = 1.1547$ ($e = 0.5$). We produce here the complete variation with μ for $1 \leqslant \mu \leqslant 3$ for the symmetric and antisymmetric states which correspond to an even angular momentum (see figures 9 and 10) (cases A and B of the appendix). The semiclassical energies were calculated only from EBK 0 in figures 11 and 12. By comparing figure 6 with figures 11 and 12 one sees that there is indeed a strong similarity in the manner in which the separatrix is crossed in the oblate cavity and in the billiard box. In both cases it is the same uniform approximation with the same phase calculated in I which is needed. Figures 11 and 12 also provide an illustration of the domain where elliptic or hyperbolic caustics are found for each quantum number. Figure 13 shows how the states are split into two components in the uniform approximation in a particular case with a high l. Such a splitting is, of course, not produced in the oblate cavity.

4. Partial wave analysis

It is interesting to perform a partial wave analysis of the wavefunctions of the cavity in order to study a possible connection between the spreading of the partial waves and the spread of the classical angular momentum.

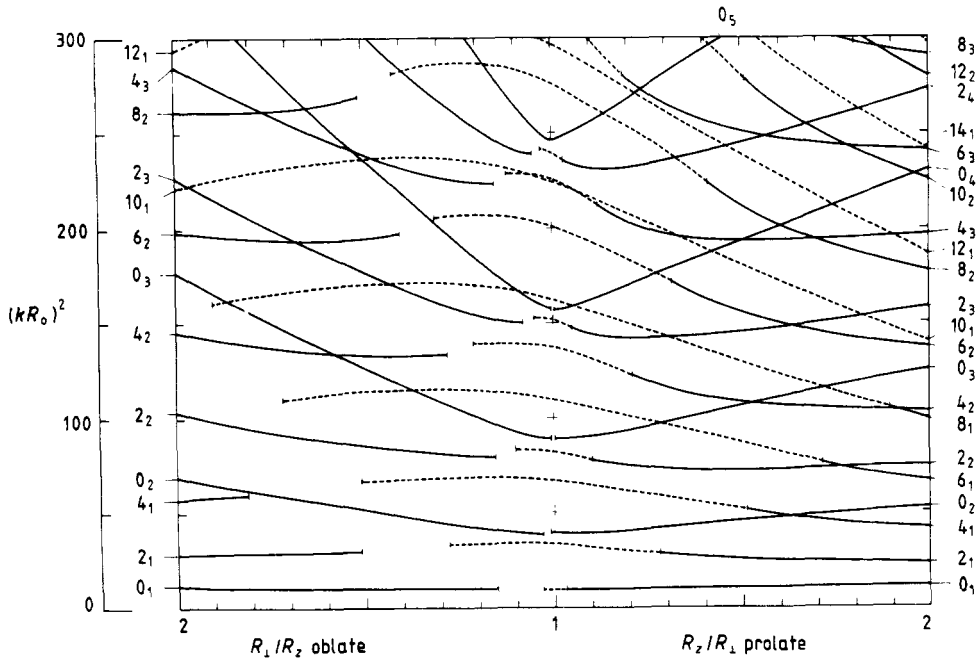

Figure 6. The complete energy spectrum of the cavities up to $(kR_0)^2 = 300$ calculated with the primitive semiclassical method. The broken curves represent when the classical caustics are elliptic, the full curves when they are hyperbolic. The gaps in the oblate case are explained by the discontinuities of the action integrals represented in the upper part of figure 2.

If a and b are, respectively, the long and short semi-axes of an elliptic caustic the classical limits for the angular momentum L_c are

$$kb \leq L_c \leq ka. \tag{41}$$

For a spherical cavity $a = b$ and there is no dispersion for the values of L_c. When μ increases a spreading of values of L_c occurs in the above interval. The lower limit kb is zero when the motion belongs to the separatrix. For higher deformations the caustics are hyperbolic and (41) is replaced by

$$0 \leq L_c \leq ka. \tag{42}$$

The signature of the separatrix is clear in the classical language: it occurs for those conditions where the lower limit of L_c is zero for the first time.

It is interesting to apply such a criterion to the spread of the l values of the quantum wavefunctions. Let $|\psi\rangle_\mu$ be any given eigenstate of the cavity that is followed as a function of μ and for which we can make the partial wave analysis

$$\langle r'|\psi\rangle_\mu = \Sigma_{n\lambda} a_{n\lambda} A_{n\lambda} j_\lambda(\alpha_{n\lambda} r') P_\lambda(\cos\theta'). \tag{43}$$

The basis of spherical Bessel functions and the change of scale defined in the appendix have been used here. The distribution of the angular momentum λ in the wavefunction $|\psi\rangle_\mu$ can be studied by considering the sums

$$b_\lambda = \Sigma_n |a_{n\lambda}|^2. \tag{44}$$

The histograms corresponding to a sample of values of μ in the interval (1.2, 2.4) are shown in figure 14 for the level $n = 1$, $l = 10$. The semiclassical limits, calculated

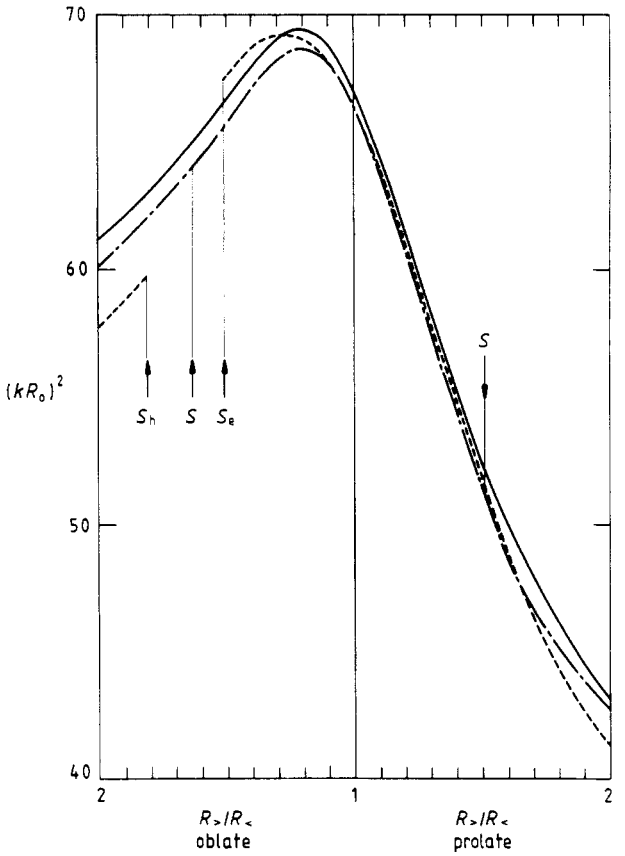

Figure 7. The semiclassical energies of the 1g state as a function of μ using the quantum equation (Q: full curve), the WKB method primitive (EBK 0: broken curve) or the uniform approximation (EBK 1: chain curve). The coordinates of the points marked S, S_e, S_h can be read in table 1 for the 1g.

with the help of (41), are represented by the arrows; the numerical values of b_0 are also given. The distribution of the b_λ is such that $b_\lambda = \delta_{\lambda 10}$ for $\mu = 1$; it spreads when $\mu \neq 1$, in principle, to all values of λ. However, it is found that b_0 becomes sufficiently large, say 10^{-2}, only in the vicinity of $\mu_S = 2.065$.

The histograms of b_λ for the 18 first excited states of the prolate cavity with $\mu = 1.5$ are represented in figure 15. The preceding behaviour of the distribution of the b_λ applies to all of them. It is remarkable that the component b_0 is important only for the states, noted with an H, which possess a hyperbolic caustic in the semiclassical theory.

5. Conclusions

The aim of this paper was to look for possible traces in the quantum spectrum of the organisation of the classical phase space and its evolution with deformation. As emphasised in the preceding paper and in § 1 the main interest of the systems that we studied is that we have three different quantum realisations of a single classical situation

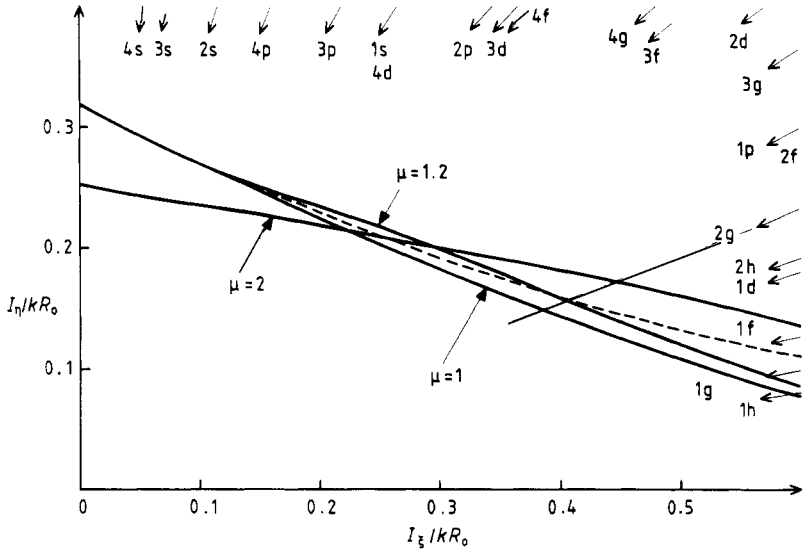

Figure 8. The energy-action surfaces are represented for $\mu = 1$, 1.2 and 2 by their intersection with the plane $kR_0 = 1$. The broken curve shows where the surface meets the separatrix for various values of μ. The arrows indicate the direction in which the semiclassical actions corresponding to the levels considered can be found.

Table 2. The values of $(kR_0)^2$ for the two components of the doublet generated from the state $n = 1$, $l = 10$ of the 'billiard'. The upper figure corresponds to the symmetric component (type 1), the lower one to the antisymmetric. The separatrix is found for $\mu_S = 2.205$ in EBK 1. On the other hand, in EBK 0 we have $\mu_{Se} = 2.025$ while $\mu_{Sh} = 2.452$ for the symmetric component and $\mu_{Sh} = 1.774$ for the antisymmetric case. These values explain why there are three levels for $\mu = 2$ in EBK 0 and only one for $\mu = 2.2$.

μ	$(kR_0)^2_Q$	$(kR_0)^2_{EBK\,0}$	$(kR_0)^2_{EBK\,1}$
1	209.5401	208.4094	208.4094
1.2	209.2714	204.9060	204.8000
	205.5224	204.9060	204.8001
1.6	186.6026	186.2705	185.2332
	187.9693	186.2705	186.5128
2	160.9155	162.7584	159.4974
		162.7584	
	170.1031	170.3125	168.4255
2.2	149.6909	missing	148.2405
	163.2567	162.1716	161.5273
2.5	135.8108	130.9285	134.3102
	155.4318	153.6399	153.6677
3	118.9417	144.4835	117.3303
	147.2758	145.2245	145.4727

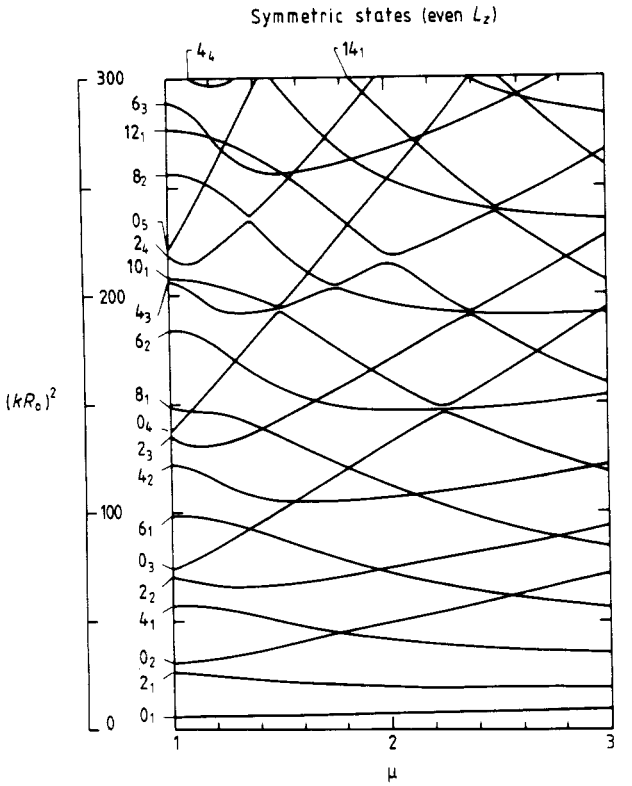

Figure 9. Quantum energy levels of the 'billiards' up to $(kR_0)^2 = 300$. The symmetric states with even L_z are shown.

with a separatrix. There is clear evidence of the crossing of the separatrix in the billiard problem. We feel that this evidence is also very striking in the even-l, odd-l differences for the oblate cavity. We have suggested that a similar effect exists also in the case of the Buck–Pilt potential in spite of its non-integrability. On the other hand, the crossing of the separatrix for the prolate cavity produces only a slight change in the curvature of the single particle energies that is observed for the even-l as well as for the odd-l. Nevertheless this event has important consequences in the partial wave analysis of the wavefunctions.

The discussion of this paper has been limited to $L_z = 0$. Its extension to other values of L_z implies the consideration of non-planar trajectories. There the difference between the prolate and the oblate cavities is even more striking because one can show that the separatrix disappears in the prolate cavity (Arvieu 1985). A discussion of this case is in progress.

Acknowledgments

One of us (RA) would like to acknowledge J Carbonell, F Brut and J Touchard for many discussions and comments during and after the course of this work. He also wants to thank M V Berry for his encouragement and his very inspiring lectures.

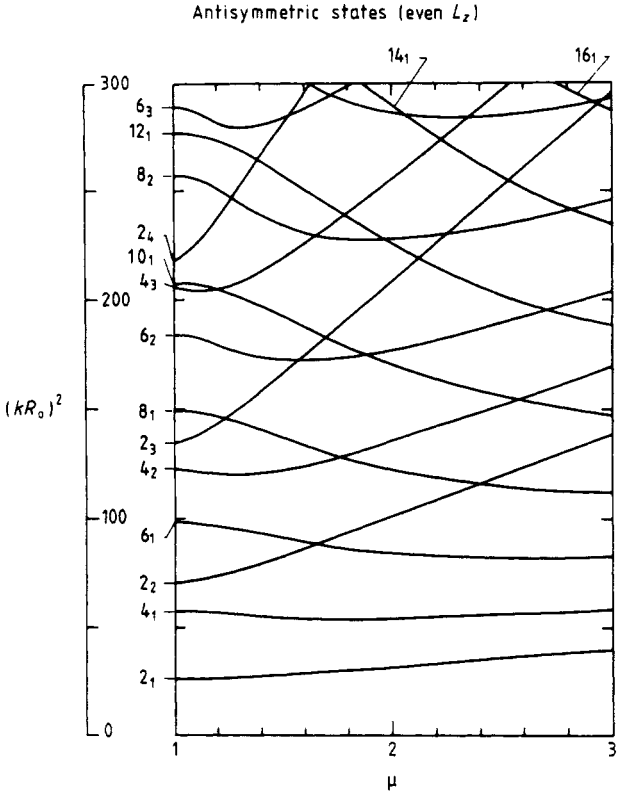

Figure 10. Same as figure 9 but for the antisymmetric states with even L_z.

Appendix

(1) 'Billiard' problem: let us define the boundary of the 'billiard' by

$$\frac{x^2}{R_\rangle^2}+\frac{y^2}{R_\langle^2}=1 \tag{A1}$$

and let us perform a scale transformation by

$$x'=\frac{R}{R_\rangle}x \qquad y'=\frac{R}{R_\langle}y. \tag{A2}$$

The wave equation becomes in the new variables

$$-\frac{\hbar^2}{2m}\Delta'\Psi-\frac{\hbar^2}{2m}\frac{R_\langle^2-R_\rangle^2}{R_\langle^2+R_\rangle^2}\left(\frac{\partial^2}{\partial x'^2}-\frac{\partial^2}{\partial y'^2}\right)\psi=\frac{\hbar^2k^2}{2m}\psi. \tag{A3}$$

The 'radius' R is defined by

$$\frac{2}{R^2}=\frac{1}{R_\rangle^2}+\frac{1}{R_\langle^2}. \tag{A2'}$$

The operator in (A3) is then written as

$$H=H_0+H_1. \tag{A4}$$

The unperturbed wavefunctions $|nm\rangle$ of H_0 are written as

$$\phi_{nm}=\langle r'|nm\rangle=A_{nm}J_m(\alpha_{nm}r')\,e^{im\phi'}. \tag{A5}$$

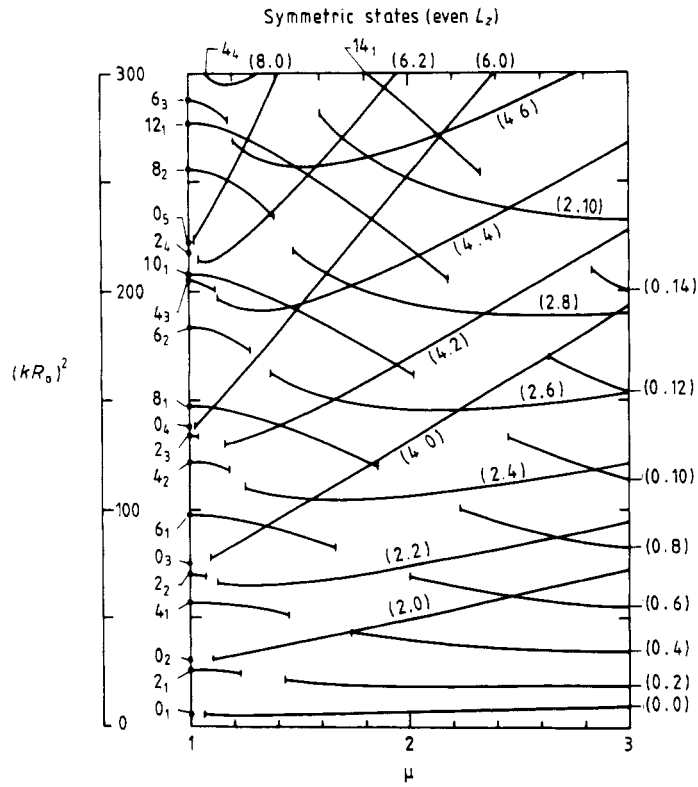

Figure 11. The levels represented in figure 9 are now calculated using the primitive WKB method. States are labelled here by the quantum number l_{n+1} for $\mu = 1$ and by (n, l) in the region after the separatrix.

ζ_{nm} is defined as the nth zero of the cylindrical Bessel function $J_m(\rho)$; α_{nm} is related to it by

$$\alpha_{nm} = \zeta_{nm}/R \tag{A6}$$

while the normalisation factor A_{nm} is equal to

$$A_{nm} = \frac{1}{\sqrt{\pi}} \frac{1}{RJ'_m(\zeta_{nm})}. \tag{A7}$$

The basis ϕ_{nm} is now used to calculate the matrix elements of H_1. However we should form four partial bases according to the parity of the states under reflection with respect to $0x$ and $0y$

(a) $\pi_x = +1$, $\pi_y = +1$; the states are denoted by $|A; nm\rangle$ with m even and positive:

$$|A; n0\rangle = |n0\rangle \tag{A8}$$

$$|A; nm\rangle = \frac{1}{\sqrt{2}}(|nm\rangle + |n-m\rangle) \qquad m > 2. \tag{A9}$$

(b) $\pi_x = -1$, $\pi_y = -1$; the states are denoted by $|B; nm\rangle$ with m even positive and $m \geq 2$:

$$|B; nm\rangle = \frac{1}{\sqrt{2}}(|nm\rangle - |n-m\rangle). \tag{A10}$$

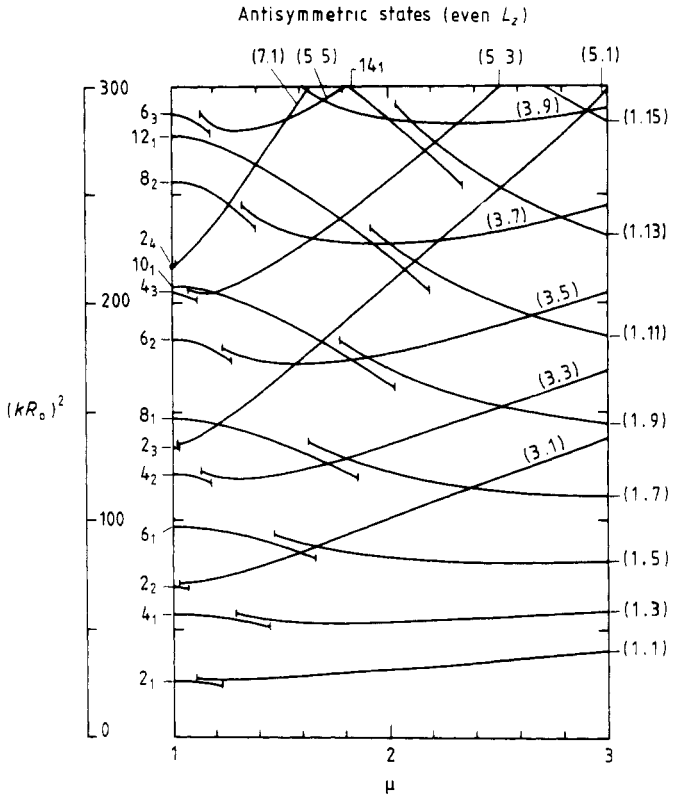

Figure 12. Same as figure 11 but for the antisymmetric states. To be compared to the exact spectrum of figure 10.

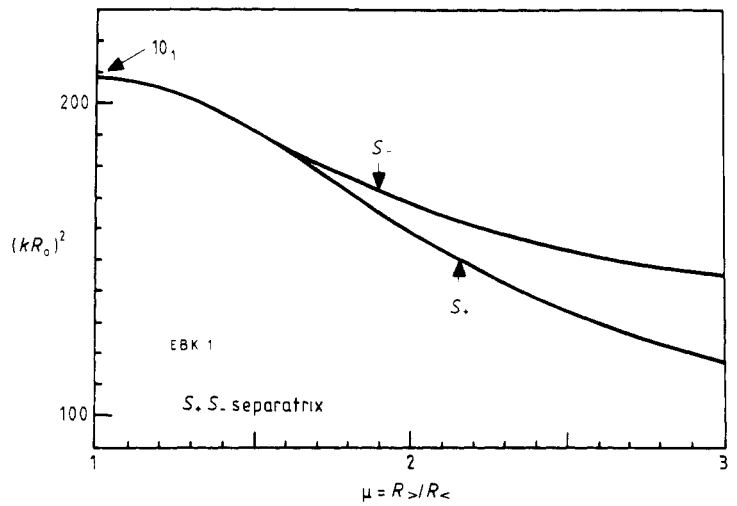

Figure 13. The splitting of the levels $n = 1$, $l = 10$ is calculated in the uniform approximation. Points where the separatrix is crossed are indicated by S_- and S_+. Since the levels almost coincide with the exact quantum levels these last results are not shown in the figure.

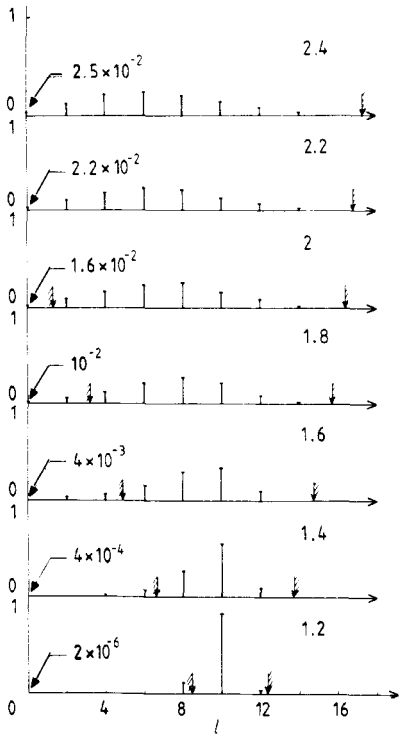

Figure 14. Distribution of the b_λ (equation (44)) with λ for the state $n_r = 1$, $l = 10$ of prolate cavities of deformations $\mu = 1.2, 1.4, \ldots, 2.4$. The vertical arrows indicate the limits (41) or (42) calculated semiclassically. The value of b_0 is explicitly given, and $\mu_c = 2.065$.

(c) $\pi_x = -1$, $\pi_y = +1$; the states are denoted by $|C; nm\rangle$ with m odd and positive:

$$|C; nm\rangle = \frac{1}{\sqrt{2}}(|nm\rangle + |n-m\rangle). \tag{A11}$$

(d) $\pi_x = +1$, $\pi_y = -1$; the states are denoted by $|D; nm\rangle$ with m odd and positive:

$$|D; nm\rangle = \frac{1}{\sqrt{2}}(|nm\rangle - |n-m\rangle). \tag{A12}$$

We define a parameter α by

$$\alpha = \frac{R_>^2 - R_<^2}{R_>^2 + R_<^2}. \tag{A13}$$

Using various recurrence relations between Bessel functions and their derivatives we can obtain (in units of $\hbar^2/2mR^2$)

$$\langle n'm+2|H_1|nm\rangle = 2\alpha(m+1)\frac{\zeta_{nm}\zeta_{n'm+2}}{\zeta_{nm}^2 - \zeta_{n'm+2}^2}. \tag{A14}$$

For $m = -1$ and $n' = n$ we should replace (A14) by

$$\langle n1|H_1|n-1\rangle = \tfrac{1}{2}\alpha\zeta_{n1}^2. \tag{A15}$$

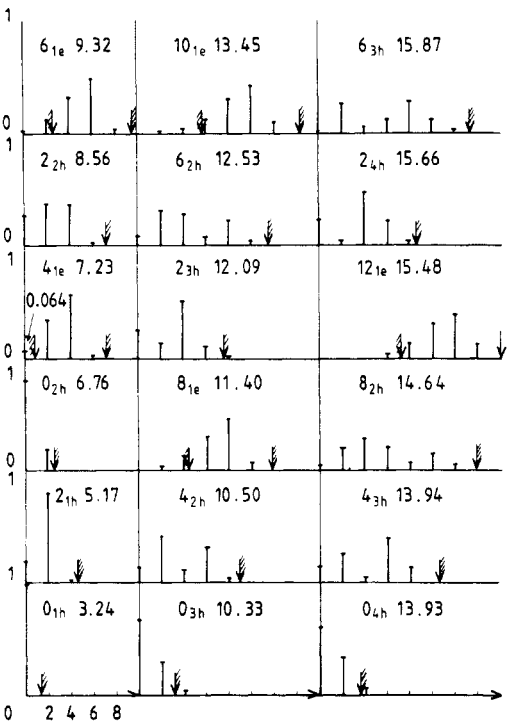

Figure 15. Distribution of the b_λ with λ for the 18 first excited states with $\mu = 1.5$. The states are denoted by l_{n+1} e or h depending on the semiclassical caustics. The arrows have the same meaning as in figure 14.

We can write the four submatrices of H_1 in the basis a, b, c and d using (A14), (A15) and the symmetry properties

$$\langle n'-m'|H_1|n-m\rangle = \langle n'm'|H_1|nm\rangle \tag{A16}$$

$$\langle n'-m-2|H_1|n-m\rangle = \langle n-m|H_1|n'-m-2\rangle = \langle n'm+2|H|nm\rangle. \tag{A17}$$

Since the unperturbed eigenvalues of H_0 are simply ζ_{nm}^2 (in units of $\hbar^2/2mR^2$) it is consistent to take all the n and l which are such that the ζ_{nl} are below a certain value in order to define a convenient basis which can be used to diagonalise H_0+H_1.

In the numerical calculation performed in this paper all the zeros below the first zero of J_{40} were included (140 zeros), among them 15 zeros of J_0, 14 of J_2, 13 of J_4, etc.

(2) Cavity: the ellipsoid is defined by

$$\frac{x^2+y^2}{R_\perp^2}+\frac{z^2}{R_z^2}=1 \tag{A18}$$

and the scale transformation as well as R are defined by

$$x'=\frac{R}{R_\perp}x \qquad y'=\frac{R}{R_\perp}y \qquad z'=\frac{R}{R_z}z \tag{A19}$$

$$\frac{3}{R^2}=\frac{2}{R_\perp^2}+\frac{1}{R_z^2}. \tag{A20}$$

The perturbation is now written in terms of a zero component of a tensor of rank two

$$H_1 = -\frac{3\hbar^2}{2m}\frac{R_\perp^2 - R_z^2}{R_\perp^2 + 2R_z^2}\left(\frac{\partial^2}{\partial z'^2} - \tfrac{1}{3}\Delta'\right). \tag{A21}$$

We now use instead of (A5) the following basis or eigenstates of L_z with $m = 0$:

$$\langle \boldsymbol{r}|nl\rangle = A_{nl} j_l(\alpha_{nl} r') P_l(\cos\theta'). \tag{A22}$$

The j_l are Bessel functions, the zeros of which are denoted by $\zeta_{nl+\frac{1}{2}}$:

$$j_l(\xi) = (\pi/2\xi)^{1/2} J_{l+1/2}(\xi) \tag{A23}$$

$$\alpha_{nl} = \zeta_{nl+1/2}/R \tag{A24}$$

$$A_{nl}^{-1} = \frac{\pi R^{3/2}}{[(2l+1)\zeta_{nl+1/2}]^{1/2}} |J'_{l+1/2}(\zeta_{nl+1/2})|. \tag{A25}$$

Using the property

$$\frac{1}{k^2}\frac{\partial^2}{\partial z^2} j_l(kr) P_l(\cos\theta)$$

$$= \frac{(l+1)(l+2)}{(2l+1)(2l+3)} j_{l+2}(kr) P_{l+2}(\cos\theta) - \frac{2l^2+2l-1}{(2l+1)(2l+3)} j_l(kr) P_l(\cos\theta)$$

$$+ \frac{l(l-1)}{(2l+1)(2l-1)} j_{l-2}(kr) P_{l-2}(\cos\theta) \tag{A26}$$

as well as properties of integrals of the Bessel functions one obtains the matrix elements of the tensor operator T_{20} defined by

$$T_{20} = \frac{\partial^2}{\partial z'^2} - \tfrac{1}{3}\Delta' \tag{A27}$$

in the basis (A22) extended to all eigenvalues m of L_z:

$$\langle n'lm|T_{20}|nlm\rangle = \delta_{nn'}\frac{2}{3R^2}\frac{\zeta_{nl+1/2}^2}{(2l-1)(2l+3)}(3m^2 - l(l+1)) \tag{A28}$$

$$\langle n'l+2m|T_{20}|nlm\rangle = -\frac{2}{R^2}\frac{\zeta_{nl+1/2}\zeta_{n'l+5/2}}{\zeta_{nl+1/2}^2 - \zeta_{n'l+5/2}^2}\frac{[((l+1)^2-m^2)((l+2)^2-m^2)]^{1/2}}{[(2l+1)(2l+5)]^{1/2}}. \tag{A29}$$

The matrix of H is decomposed into two submatrices according to the parity (-1).

Again the classification of the unperturbed states by the values of $\zeta_{nl1/2}^2$ is necessary. The calculations reported in this paper correspond to a basis of 86 states of positive parity (12 states $l = 0$, 11 states $l = 2$, etc, up to 4 states $l = 20$) and 78 states of negative parity (12 states $l = 1$, etc, up to 4 states $l = 19$). This calculation would correspond in the usual nuclear shell model language with harmonic oscillator wavefunctions to 24 shells of the harmonic oscillator.

(3) Accidental degeneracies: the quantum spectrum that we have calculated and which is represented by figures 3, 10 and 11, exhibits a certain number of crossings. Since we have not found out an analytic formula, the real existence of these crossings does not rely upon a theoretical analysis. It is, however, possible to show that the levels of a separable system may cross. We have been able to prove numerically the existence of a few of our crossings. However an analysis such as that given by Berry on the crossing of the triangle is still lacking and is not included in our study.

References

Arvieu R 1985 *Proc. topical meeting on 'Phase Space Approach to Nuclear Dynamics' ICTP, Trieste* ed M di Toro, W Nörenberg, M Rosina and M Stringan (Singapore: World Scientific) p 509
Ayant Y and Arvieu R 1987 *J. Phys. A: Math. Gen.* **20** 397-409
Carbonell J 1983 *Thèse de 3ème cycle* Université de Grenoble
Carbonell J, Brut F, Arvieu R and Touchard J 1984 *J. Physique Coll.* **45** 371-8
—— 1985 *J. Phys. G: Nucl. Phys.* **11** 325-42
Ford K W, Hill D L, Wakano M and Wheeler J A 1959 *Ann. Phys., NY* **7** 239-58
Keller J B and Rubinow S I 1960 *Ann. Phys., NY* **9** 24-75
Touchard J 1985 private communication
Moszkowski S A 1955 *Phys. Rev.* **99** 803-9